


A quantum cascade laser-pumped molecular laser tunable over 1 THz


Cite as: APL Photonics **7**, 016107 (2022); <https://doi.org/10.1063/5.0076310>

Submitted: 23 October 2021 • Accepted: 06 January 2022 • Accepted Manuscript Online: 06 January 2022 • Published Online: 25 January 2022

Arman Amirzhan,  Paul Chevalier, Jeremy Rowlette, et al.

COLLECTIONS

 This paper was selected as Featured

 This paper was selected as Scilight



View Online



Export Citation



CrossMark

ARTICLES YOU MAY BE INTERESTED IN

[Quantum communication with time-bin entanglement over a wavelength-multiplexed fiber network](#)

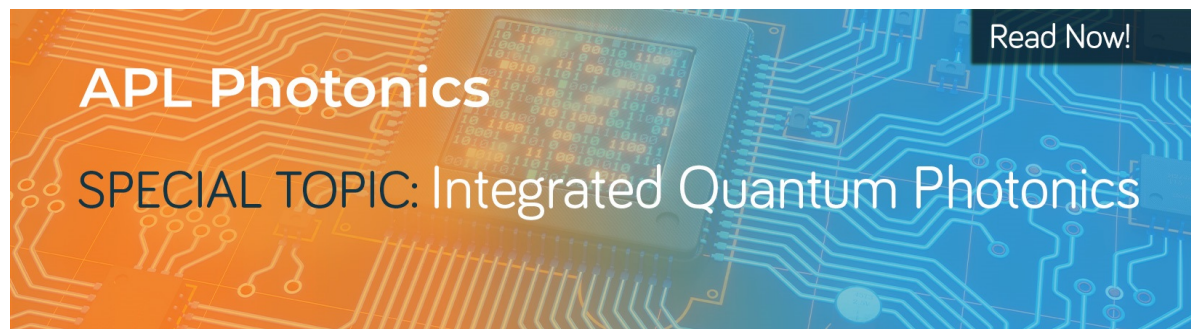
APL Photonics **7**, 016106 (2022); <https://doi.org/10.1063/5.0073040>

[A perspective on twisted light from on-chip devices](#)

APL Photonics **6**, 110901 (2021); <https://doi.org/10.1063/5.0060736>

[Toward robust and practical interband cascade laser frequency combs: A perspective](#)

Applied Physics Letters **119**, 230503 (2021); <https://doi.org/10.1063/5.0069548>



A quantum cascade laser-pumped molecular laser tunable over 1 THz

Cite as: APL Photon. 7, 016107 (2022); doi: 10.1063/5.0076310

Submitted: 23 October 2021 • Accepted: 6 January 2022 •

Published Online: 25 January 2022



Arman Amirzhan,¹ Paul Chevalier,¹  Jeremy Rowlette,² H. Ted Stinson,² Michael Pushkarsky,² Timothy Day,² Henry O. Everitt,^{3,4,a)}  and Federico Capasso^{1,a)} 

AFFILIATIONS

¹ Harvard John A. Paulson School of Engineering and Applied Sciences, Harvard University, Cambridge, Massachusetts 02138, USA

² DRS Daylight Solutions, San Diego, California 92128, USA

³ DEVCOM Army Research Laboratory, Houston, Texas 77005, USA

⁴ Department of Physics, Duke University, Durham, North Carolina 27708, USA

^{a)} Authors to whom correspondence should be addressed: everitt@phy.duke.edu and capasso@seas.harvard.edu

ABSTRACT

Despite decades of research, no frequency tunable sources span the terahertz gap between 0.3 and 3 THz. By introducing methyl fluoride (CH_3F) as a new gain medium for a quantum cascade laser-pumped molecular laser (QPML), we demonstrate continuous-wave lasing from more than 120 discrete transitions, spanning the range from 0.25 to 1.3 THz. Thanks to its large permanent dipole moment and large rotational constants, methyl fluoride (CH_3F) as a QPML gain medium combines a lower threshold, a larger power efficiency, and a wider tuning range than other molecules. These key features of the CH_3F QPML, operated in a compact cavity at room temperature, pave the way to a versatile THz source to bridge the THz gap.

© 2022 Author(s). All article content, except where otherwise noted, is licensed under a Creative Commons Attribution (CC BY) license (<http://creativecommons.org/licenses/by/4.0/>). <https://doi.org/10.1063/5.0076310>

As terahertz (THz) technologies mature and create exciting applications in radio astronomy,¹ biomedicine,² communications, and the defense/aerospace industries,³ the generation and detection of THz radiation remains a challenge. Despite decades of extensive research in the area, few practical sources of THz radiation exist. Vacuum electronic devices and multiplier chain sources struggle to reach frequencies above 1 THz, free-electron lasers and optically pumped far-infrared (IR) lasers (OPFIR) are bulky and non-portable, and difference frequency photomixers produce broad linewidths and low output power.⁴ THz quantum cascade lasers, despite recent advances, can operate only in pulsed mode using thermoelectric coolers⁵ and require cryogenic cooling for cw operation.⁶

A new source of widely tunable THz radiation has been recently demonstrated: the Quantum Cascade Laser (QCL) pumped molecular laser (QPML).^{7–9} The QPML, a new class of OPFIR lasers,^{10,11} requires the pumping of a mid-IR rovibrational transition with an external laser to create population inversions in dipole-allowed transitions between adjacent rotational energy levels, with lasing

frequencies in the THz range. The advantage of the QPML concept is that it uses a compact, continuously tunable mid-IR QCL as a pumping source instead of a bulky, line-tunable mid-IR gas laser. The latter requires a frequency coincidence between a CO_2 laser line and a mid-IR rovibrational transition to produce lasing on one or two, often unfavorable, THz rotational transitions. To change OPFIR laser frequency, the user has to change the molecular gain medium and the pump laser line. By contrast, the continuous tunability of QCLs allows *any* rovibrational transition to be pumped for *any* gas-phase molecules with a permanent electric dipole moment, so the challenge is to identify the ideal molecular gain medium that provides the best combination of power and tunability. Then, placing this molecular gain medium in a small laser cavity^{11,12} will create a room temperature cw laser in a compact form factor with the potential for wide frequency tunability throughout the THz region.

We have previously demonstrated the widely tunable QPML concept by using an external cavity QCL as a pump source and nitrous oxide (N_2O) as a molecular gain medium, achieving

low-power continuous-wave laser emission for 39 transitions with discrete line tunability from 0.25 to 0.95 THz.⁸ The first demonstration of a QPML used ammonia gas molecules (NH_3) as a gain medium⁷ and was based on population inversion of pure inversion transitions in the $\nu_2 = 1$ excited vibration band. Such pure inversion transitions can achieve higher output power, with more than 1 mW demonstrated recently¹³ but with a tuning range limited to a few frequencies between 0.9 and 1.1 THz. Another QPML demonstration using ammonia produced five more lasing lines in the range from 4.4 to 4.5 THz using direct rotational transitions in the same $\nu_2 = 1$ exciting vibration.⁹

Here, we introduce methyl fluoride (CH_3F) as the most promising gas-phase QPML molecular gain medium to date, by demonstrating lasing from more than 120 of the 315 possible lines, spanning the frequency range 0.25–1.3 THz, and always producing at least 10 times more output power than from the N_2O QPML operating at the nearest emission frequency. Laser emission beyond 1 THz

is reliably achieved, thanks to larger rotational constants and a lower lasing threshold at the optimal working pressure. The low lasing threshold and the high power efficiency of the CH_3F QPML permitted by the molecule's large permanent dipole moment make it suitable for applications even with the QCL pump emitting as little as 50 mW. Thanks to its compactness, efficiency, wide tuning range, and room temperature operation, the methyl fluoride QPML has the potential to become a key technology to bridge the THz gap from 200 GHz up to 2 THz for applications in imaging, security, or communications.

Methyl fluoride is a prolate symmetric top molecule [see Fig. 1(a) inset] whose rovibrational energy level structure is characterized by two quantum numbers: J , representing the total angular momentum, and K , representing the projection of the angular momentum along the main symmetry axis. The energies of the rotational states within a given vibrational energy band, up to the fourth order in J and K , are given by¹⁷

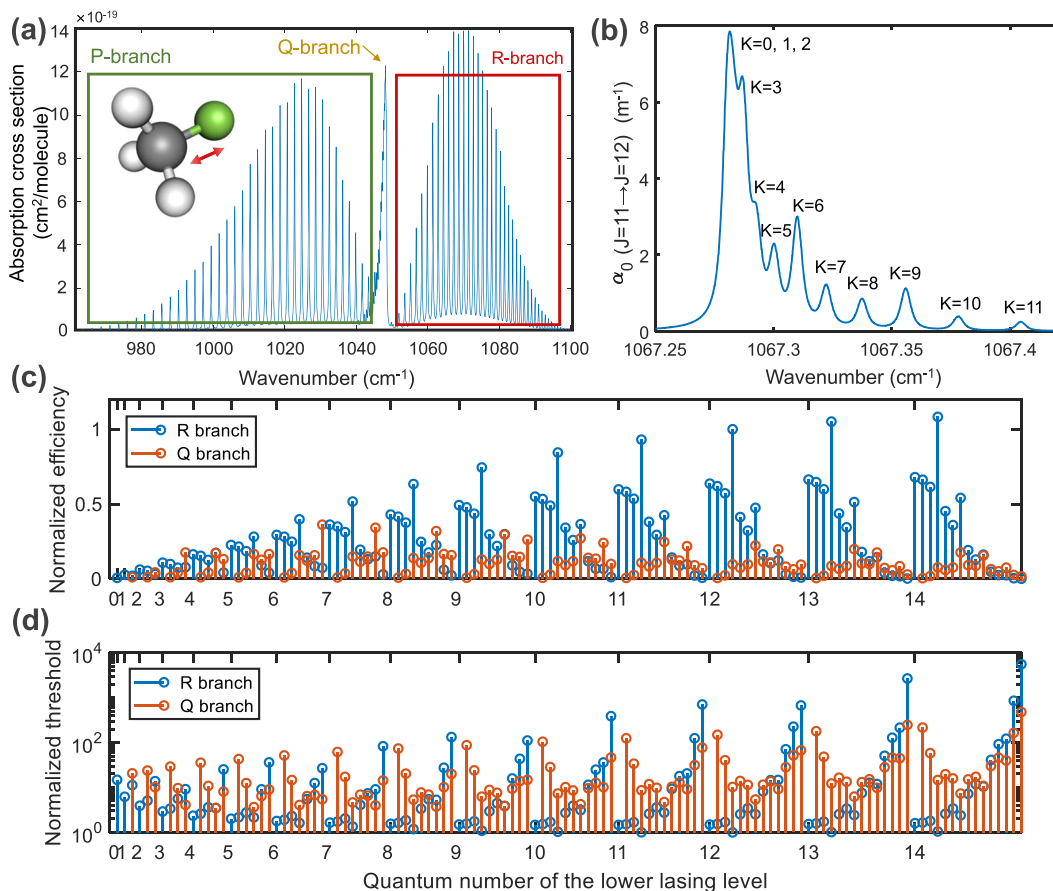


FIG. 1. (a) Room-temperature IR spectrum of the $\nu_3 = 1$ rovibrational band of CH_3F around 1000 cm^{-1} , showing the absorption cross sections as a function of wavenumber for the P-, Q-, and R-branch transitions, using data obtained from the HITRAN database.^{14,15} (b) Simulated room temperature spectrum of the Doppler-broadened R-branch rovibrational transitions from the $J_L = 11$ ground vibrational level at 30 mTorr, using Ref. 16. Estimated relative power efficiency (c) and threshold (d) plotted as a function of lower laser level $J_U - 1$ and K , normalized by the respective values for the $J = 13 \rightarrow 12$, $K = 3$ transition. For a Q-branch pump, $J_U - 1 = J_L - 1$, and for an R-branch pump, $J_U - 1 = J_L$.

$$F(J, K) = BJ(J+1) + (A-B)K^2 - D_J J^2(J+1)^2 - D_{JK}J(J+1)K^2 - D_K K^4, \quad (1)$$

where B and A are rotational constants, and D_J , D_{JK} , and D_K are centrifugal distortion constants, unique for each vibrational energy band. A more thorough polynomial development is given in the [supplementary material](#). As methyl fluoride is a prolate symmetric top molecule, its rotational constant A (≈ 150 GHz) is larger than B (≈ 25 GHz),¹⁶ so the energy of rotational states increases with increasing J and K . Given the dipole-allowed $\Delta J = 0, \pm 1, \Delta K = 0$ transition selection rules,¹⁷ the laser transition frequency between adjacent rotational energy states can be calculated using Eq. (1) to be

$$\begin{aligned} \nu(J, K) &= F(J+1, K) - F(J, K) \\ &= 2B(J+1) - 4D_J(J+1)^3 - 2D_{JK}(J+1)K^2. \end{aligned} \quad (2)$$

Our QCL frequency can be tuned across the lowest energy ν_3 vibrational band of CH_3F ,¹⁶ whose IR spectrum is shown in Fig. 1(a) and whose carbon–fluorine stretching is illustrated in the inset. This molecular gain medium is pumped from a ground-state rotational level with quantum numbers J_L, K_L to a rotational state in the $\nu_3 = 1$ vibrational level with quantum numbers J_U, K_U . The CH_3F gain medium was pumped either with an R-branch transition ($J_U = J_L + 1, K = K_U = K_L$) or with a Q-branch transition ($J_U = J_L, K = K_U = K_L \neq 0$). P-branch IR transitions could have been pumped too, but they are so similar to R-branch transitions, except for their frequency, that they were not considered here. The number of allowed IR transitions between a given $J_L \rightarrow J_U$ increases with increasing J_L , spanning $K = 0, 1, \dots, J_L$ with frequencies that separate quadratically with K because of centrifugal distortion [Eq. (2)], as can be seen in Fig. 1(b). Because the IR branching ratio transition matrix element is proportional to $\frac{(J+1)^2 - K^2}{(J+1)(2J+1)}$ for R-branch transitions and to $\frac{K^2}{J(J+1)}$ for Q-branch transitions,¹⁷ R-branch pumping favors low K transitions, and Q-branch pumping is more effective for high K transitions.

A rotational population inversion can occur within the $\nu_3 = 1$ vibrational state between levels with quantum numbers J_U and $J_U - 1$. Because the emission frequency from Eq. (2) depends on K , for a given J_U , there are J_U possible laser transitions ($K = 0$ to $J_U - 1$) for R-branch pumping and $J_U - 1$ ($K = 1$ to $J_U - 1$) for Q-branch pumping. It is this increasing number of discrete laser lines with increasing J_U , coupled with the ability to pump either R- or Q-branch transitions with a single QCL to maximize power, which makes CH_3F an attractive gain medium for high tunability, and is achieved by selectively pumping rovibrational transitions of different K values.

The THz emission power and lasing threshold of the CH_3F QPML, which can be estimated using a comprehensive model¹² that considers all molecular relaxation mechanisms, can be reasonably approximated by a far simpler model^{8,18} in the low-pressure regime where the rate of unfavorable molecular dipole–dipole collisions is smaller than the rate of favorable hard collisions with the cavity walls. The salient expressions, recalled in the [supplementary material](#), indicate that at a given frequency, the output

power increases, and the lasing threshold decreases with increasing absorption strength of the pumped IR transition.

Although actual laser power and threshold sensitively depend on cavity geometry and loss, the simple model thereby indicates that one may ascertain the relative efficacy of the allowed laser transitions when pumped by P-, Q-, or R-branch transitions by comparing their relative IR absorption strengths. For thermally populated rotational energy levels (*i.e.* $F(J, K) < kT$) in ν_0 , these can be easily calculated (see the [supplementary material](#)) using Eq. (1) and the known degeneracies to estimate the fractional occupation of J_L, K_L , multiplied by the branching ratio for the considered IR pumping branch (P, Q, or R). Likewise, the relative power efficiency may be estimated by multiplying the relative IR absorption by J_U to account for the frequency dependence of the laser transition, while the relative lasing threshold may be estimated by multiplying the relative IR absorption by the branching ratio for the lasing transition.

For the CH_3F QPML, the efficiency and the lasing threshold for many of these lines are compared for both R- and Q-branch pumping in Figs. 1(c) and 1(d), respectively, as a function of the lower lasing level quantum numbers $J_U - 1$. For a Q-branch pump, $J_U - 1 = J_L - 1$, and for an R-branch pump, $J_U - 1 = J_L$. The plots in Figs. 1(c) and 1(d) have been, respectively, normalized to the efficiency and threshold of the lasing line with the lowest lasing threshold ($J = 13 \rightarrow 12, K = 3$). Notice that the lowest thresholds generally occur for low K lines when pumped by R (and P) branch transitions but for mid-range K lines when pumped by Q-branch transitions. Likewise, the highest power efficiencies generally occur for $K = 3$ lines when pumped by R (or P) branch transitions and $K = 6$ lines for Q-branch pumping. This simple analysis provides an easy way to compare the performance of the many allowed laser transitions from a QPML with a symmetric top molecular gain medium, allowing one to ascertain the most efficient and the lowest threshold lasing lines.

Figure 2 shows a simplified schematic of the experimental setup, and a more detailed schematic is shown in the [supplementary material](#). The IR pump is provided by an external cavity (EC)-QCL (Daylight Solutions 41095-HHG-UT, tunable from 920 to 1194 cm^{-1}) emitting up to 250 mW. The THz cavity is a copper pipe with a 4.8 mm internal diameter and 50 cm in length. A flat mirror with a centered 1-mm diameter pinhole was used as the output coupler. The cavity resonance frequency was tuned by changing the tuning mirror position to adjust the cavity length.

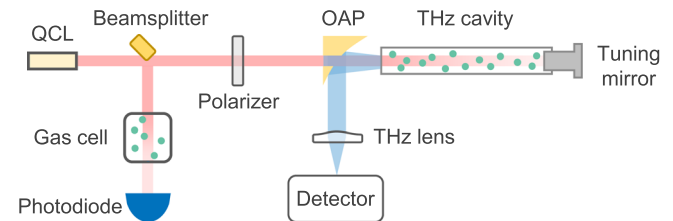


FIG. 2. Schematic of the experimental setup. A gold-plated silicon wafer was used as a beamsplitter to reflect a small portion (about 5% of the incoming power) of the pump beam into the reference gas cell, while the rest entered the THz cavity. The following detectors were used to detect lasing lines: Schottky diodes between 0.25 and 1.1 THz, a Golay cell above 1.1 THz, and heterodyne receivers to measure spectra between 0.3 and 1.1 THz.

A separate CH_3F gas absorption cell was used to monitor how precisely the QCL emission frequency was tuned to the desired CH_3F rovibrational transition. About 5% of the incoming power was sampled and redirected toward this gas cell by using a small piece of a gold-coated silicon wafer that partially clipped the edge of the QCL beam.

The QCL pump beam was coupled into the THz laser cavity through the pinhole in the output coupler using an anti-reflective coated ZnSe lens to focus the beam into the pinhole. A 2-mm-thick ZnSe window mounted at the Brewster angle was used to maximize the amount of QCL power injected into the vacuum-tight gas laser cavity. A wire grid polarizer mounted on a rotational stage was used

as a variable attenuator for the linearly polarized QCL beam. The injected IR power was measured by replacing the QPML rear tuning mirror with a ZnSe window and measuring the pump beam power transmitted through the THz cavity. After passing through the coupling optics, the maximum power transmitted through the cavity was measured to be about 150 mW at 1065 cm^{-1} .

The off-axis parabolic mirror (OAP) used to collect the generated THz laser radiation had a hole drilled along the focal axis through which the pump beam was coupled into the THz laser cavity. A polytetrafluoroethylene (PTFE) lens blocked any residual IR signal and focused the collected THz beam onto a Schottky diode detector, a Golay cell, or a heterodyne receiver. The THz

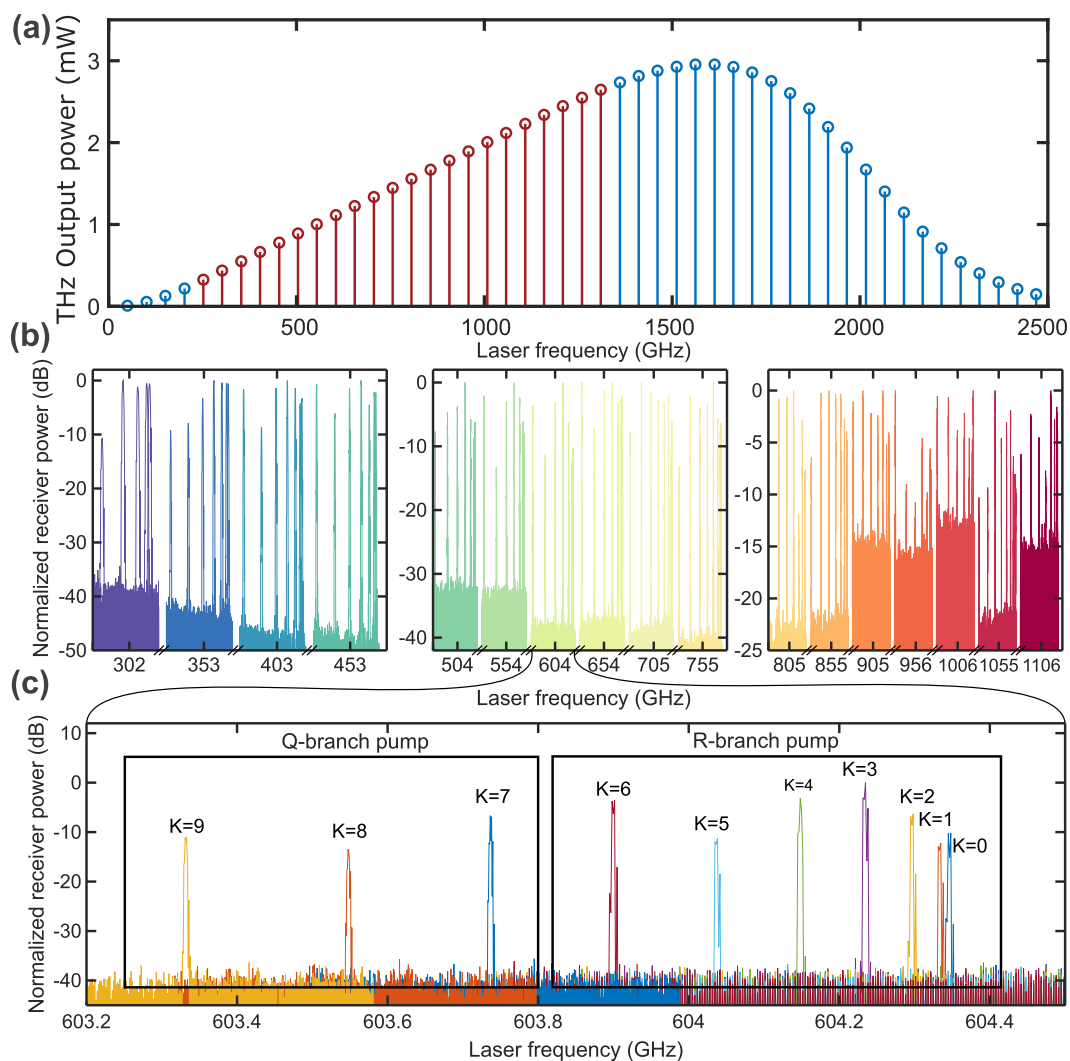


FIG. 3. (a) Plot of estimated maximum THz emission power using a simple model¹⁸ for a 30 Torr CH_3F QPML pumped with a 150 mW QCL, as a function of the frequency for a 4.8 mm diameter, 50 cm long cell. Red lines represent transitions at which laser emission was attempted and achieved. Blue lines represent transitions at which laser emission is theoretically possible but was either not achieved or not attempted. (b) Experimental data showing all lines measured using a heterodyne receiver, from 302 to 1106 GHz. (c) Detailed view of measured lasing lines emitting around 603 GHz, showing which lines were pumped with an R- or Q-branch transition.

output power was measured using a calibrated calorimeter-style power meter (VDI PM5B).

The theoretically predicted output power of a CH_3F QPML pumped by a 150 mW QCL with a gas pressure of 30 mTorr is plotted in Fig. 3(a). This plot was obtained using the enhanced simple model previously mentioned¹⁸ that takes into account dipole–dipole collisions, multiple passes of the infrared pump, but for that particular plot, no infrared saturation was considered. The output power was calculated as a function of the laser frequency, assuming that the gain medium was pumped using an R-branch transition with $J_L = 1$ –50 and $K = 3$ (except for $J_L \leq 3$ where $K = 0$ was assumed). Maximum QPML power is expected between 1 and 1.7 THz.

Laser emission was obtained experimentally by tuning the QCL into coincidence with a Q- or R-branch rovibrational transition of the gain medium and then by tuning the cavity resonance into coincidence with the lasing rotational transition by adjusting the cavity length with a differential micrometer screw (Newport DM17-4, 100 nm fine sensitivity) of a translation stage. Emission was achieved on lines between 0.25 and 1.3 THz by pumping rovibrational transitions of CH_3F originating from a level with quantum number J_L spanning from 5 to 25 and various K numbers. Of the 315 possible lasing lines over this range, pumping was attempted and emission was observed for at least 120 of them [shown as red lines on Fig. 3(a)], including many measured using a heterodyne receiver that are plotted together in Fig. 3(b). The blue lines in Fig. 3(a) represent transitions for which laser emission is possible but was either not attempted (for frequencies above 1.3 THz) or was not possible in our laser cavity (for frequencies below 250 GHz). In Fig. 3(c), a detailed view of lasing lines obtained around 604 GHz is shown, indicating which lines were pumped by an R-branch transition or a Q-branch transition. As anticipated, lines with a larger K quantum number were more efficiently pumped with Q-branch transitions, while the lines with a lower K quantum number were more efficiently pumped with R-branch transitions. Because the lower K lines are spectrally close together, we were routinely able to induce two, three, and even four transitions to lase simultaneously with R-branch pumping.

The output power of the THz laser emission depends on a combination of many parameters, including the choice of the gain medium, the IR pumping efficiency, and the laser cavity design.¹⁸ The choice of the gain medium will be motivated by many properties, including its IR absorption coefficient and saturation, the dipole moments of the lasing transitions, the dipole–dipole collision rate, and the ratio of the emission frequency to the pump frequency. The pumping efficiency will be primarily affected by the available QCL power and the overlap between the QCL emission linewidth and the gain medium absorption bandwidth. The effects of the laser cavity are determined by its geometry, cavity quality factor, loss factor of pump power inside the cavity, and the THz losses in the output coupler. All the above factors must be considered in calculating the optimum THz cavity length, diameter, output coupling ratio, and gas pressure.¹⁸ Increasing the cavity diameter results in improved cavity Q factor and reduced pump saturation, but at the expense of increased inversion–quenching caused by the reduced relaxation rate through wall collisions. Optimal cavity dimensions, operating pressure, and more accurate output powers are calculated by performing extensive molecular dynamics simulations.^{12,18}

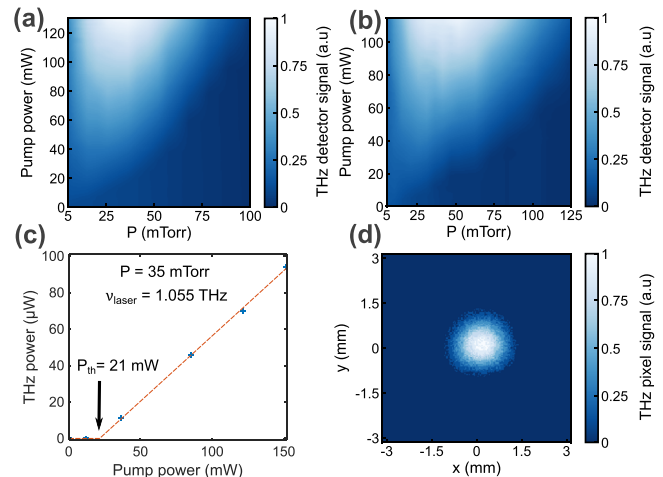


FIG. 4. Experimental data showing the detected THz power as a function of gas pressure and IR pump power for emission near (a) 604 GHz and (b) 1.1 THz. (c) Output power vs pump power curve obtained with a gas pressure of 35 mTorr for the $J = 21 \rightarrow 20$, $K = 3$ transition at 1.055 THz. (d) Profile of the THz focused spot for the same transition measured with a microbolometer camera.

The laser performance has been measured experimentally at various gas pressures and pump powers. The experiment was conducted by setting the pressure to a fixed value and then slowly adjusting the QCL pump power while measuring the THz signal strength using a Schottky diode detector. By referencing the measured signal strength against the largest measured power for a given lasing transition, a surface plot of normalized THz output signal as a function of pump power and pressure can be constructed, such as shown in Fig. 4(a) for the $J = 12 \rightarrow 11$, $K = 3$ lasing transition near 604 GHz and in Fig. 4(b) for the $J = 22 \rightarrow 21$, $K = 3$ lasing transition near 1.1 THz. The threshold increases with increasing pressure because of the pressure-dependent dipole–dipole collision rate that operates to quench the inversion.¹⁸ The pressure for optimal power increases with increasing pump power as expected, but it also increases with increasing THz emission frequency, from ~30 mTorr for 604 GHz to ~50 mTorr for 1.1 THz. This occurs because above $J_L = 11$, the fractional population decreases with increasing J_L , thereby requiring more pressure to avoid pump saturation and achieve comparable IR absorption strength.

Comparing different laser transitions, the largest THz output power occurs when the highest population inversion is obtained, determined primarily by the absorption strength of the pumped transition and the lasing frequency to pump frequency ratio. Consequently, the output power will vary significantly with THz emission frequency, as shown in Fig. 3(a). The largest measured THz power (13 μW) was obtained for the $J = 12 \rightarrow 11$, $K = 3$ transition near 604 GHz for a pump power of 145 mW at a pressure of 30 mTorr. Because the QPML is increasingly sensitive to cavity misalignment with increasing frequency, more power was measured at 604 GHz than at 1.055 THz, a problem that will be overcome with improved cavity design. About 9.5 μW of collected power was measured at

around 1.055 THz (for the $J = 21 \rightarrow 20$, $K = 3$ transition) for a pump power of 150 mW at a pressure of 35 mTorr.

The laser power collection efficiency through the ZnSe Brewster window, the off-axis parabolic mirror, and the PTFE lens was experimentally estimated at most at 10%, which corresponds to a total emitted power of at least 130 μ W at 604 GHz and at least 95 μ W at 1.055 THz. The normalized power efficiency (defined by the power efficiency divided by the ratio of the emitted photon energy by the pump photon energy) is 4.7% at 604 GHz and 2% at 1.055 THz. These power efficiencies compare favorably with the performance of commercial OPFIR lasers, and greater efficiency approaching the theoretical maximum of 50% is possible with improved cavity design and alignment.¹⁸

The estimated emitted THz power as a function of pump power for the 1.055 THz transition is plotted in Fig. 4(c), where the collected power was measured for five different pump power values (blue crosses); the red-dashed line is a linear fit of the THz power above the threshold. A clear threshold of around 21 mW pump power can be seen. The profile of the laser spot, as focused by the PTFE lens for the same transition, was measured using a microbolometer camera (INO Microxcam 384i-THz) and is shown in Fig. 4(d). The spot was fitted with a two-dimensional Gaussian model with spot sizes $2w_x = 2.08$ mm and $2w_y = 1.89$ mm.

In summary, we have shown that by using a widely tunable external cavity quantum cascade laser to pump gaseous methyl fluoride, a prolate symmetric top molecule with a large dipole moment and rotational constant created a widely tunable THz lasing over many lasing lines can be achieved. It is this wide tunability, coupled with its low threshold, ability to pump either R- or Q-branch transitions to maximize power, good conversion efficiency, high operating frequency, and compact size, which make QPML's in general and the CH₃F QPML in particular, a leap-ahead source technology for generating THz radiation.^{7–9}

See the [supplementary material](#) for additional details about the experimental and theoretical work presented in this manuscript.

The external cavity QCL used in the experiments was provided by DRS Daylight Solutions. The authors acknowledge Stanley Cotreau and Andrew DiMambro of the Harvard University Instructional machine shop for their help with the fabrication of the THz cavity elements. This work was partially supported by the U.S. Army Research Office (Contract Nos. W911NF-19-2-0168 and W911NF-20-1-0157). Any opinions, findings, conclusions, or recommendations expressed in this material are those of the authors and do not necessarily reflect the views of the Assistant Secretary of Defense for Research.

AUTHOR DECLARATIONS

Conflict of Interest

The authors declare no conflicts of interest.

Author Contributions

A.A. and P.C. contributed equally to this work.

DATA AVAILABILITY

The data that support the findings of this study are available from the corresponding authors upon reasonable request.

REFERENCES

- 1 A. Wootten and A. R. Thompson, "The atacama large millimeter/submillimeter array," *Proc. IEEE* **97**, 1463–1471 (2009).
- 2 Q. Sun, Y. He, K. Liu, S. Fan, E. P. J. Parrott, and E. Pickwell-MacPherson, "Recent advances in terahertz technology for biomedical applications," *Quant. Imaging Med. Surg.* **7**, 345 (2017).
- 3 F. Ellrich, M. Bauer, N. Schreiner, A. Keil, T. Pfeiffer, J. Klier, S. Weber, J. Jonuscheit, F. Friederich, and D. Molter, "Terahertz quality inspection for automotive and aviation industries," *J. Infrared, Millimeter, Terahertz Waves* **41**, 470–489 (2020).
- 4 E. Bründermann, H.-W. Hübers, and M. F. Kimmitt, "Sources," in *Terahertz Techniques* (Springer, 2012), pp. 103–168.
- 5 A. Khalatpour, A. K. Paulsen, C. Deimert, Z. R. Wasilewski, and Q. Hu, "High-power portable terahertz laser systems," *Nat. Photonics* **15**, 16–20 (2021).
- 6 M. Wienold, B. Röben, L. Schrottke, R. Sharma, A. Tahraoui, K. Biermann, and H. T. Grah, "High-temperature, continuous-wave operation of terahertz quantum-cascade lasers with metal-metal waveguides and third-order distributed feedback," *Opt. Express* **22**, 3334–3348 (2014).
- 7 A. Pagies, G. Ducournau, and J.-F. Lampin, "Low-threshold terahertz molecular laser optically pumped by a quantum cascade laser," *APL Photonics* **1**, 031302 (2016).
- 8 P. Chevalier, A. Amirzhan, F. Wang, M. Piccardo, S. G. Johnson, F. Capasso, and H. O. Everitt, "Widely tunable compact terahertz gas lasers," *Science* **366**, 856–860 (2019).
- 9 M. Wienold, A. Zubairova, and H.-W. Hübers, "Laser emission at 4.5 THz from ¹⁵NH₃ and a mid-infrared quantum-cascade laser as a pump source," *Opt. Express* **28**, 23114–23121 (2020).
- 10 T. Y. Chang and T. J. Bridges, "Laser action at 452, 496, and 541 μ m in optically pumped CH₃F," *Opt. Commun.* **1**, 423–426 (1970).
- 11 H. O. Everitt, D. D. Skatrud, and F. C. DeLucia, "Dynamics and tunability of a small optically pumped cw far-infrared laser," *Appl. Phys. Lett.* **49**, 995–997 (1986).
- 12 F. Wang, J. Lee, D. J. Phillips, S. G. Holliday, S.-L. Chua, J. Bravo-Abad, J. D. Joannopoulos, M. Soljačić, S. G. Johnson, and H. O. Everitt, "A high-efficiency regime for gas-phase terahertz lasers," *Proc. Natl. Acad. Sci. U. S. A.* **115**, 6614–6619 (2018).
- 13 J.-F. Lampin, A. Pagies, G. Santarelli, J. Hesler, W. Hansel, R. Holzwarth, and S. Barbieri, "Quantum cascade laser-pumped terahertz molecular lasers: Frequency noise and phase-locking using a 1560 nm frequency comb," *Opt. Express* **28**, 2091–2106 (2020).
- 14 R. Kochanov, I. Gordon, L. Rothman, K. Shine, S. Sharpe, T. Johnson, T. Wallington, J. Harrison, P. Bernath, M. Birk, G. Wagner, K. L. Bris, I. Bravo, and C. Hill, "Infrared absorption cross-sections in HITRAN2016 and beyond: Expansion for climate, environment, and atmospheric applications," *J. Quant. Spectrosc. Radiat. Transfer* **230**, 172 (2019).
- 15 S. W. Sharpe, T. J. Johnson, R. L. Sams, P. M. Chu, G. C. Roderick, and P. A. Johnson, "Gas-phase databases for quantitative infrared spectroscopy," *Appl. Spectrosc.* **58**, 1452–1461 (2004).
- 16 D. J. Phillips, E. A. Tanner, F. C. De Lucia, and H. O. Everitt, "Infrared-terahertz double-resonance spectroscopy of CH₃F and CH₃Cl at atmospheric pressure," *Phys. Rev. A* **85**, 052507 (2012).
- 17 C. H. Townes and A. L. Schawlow, *Microwave Spectroscopy* (Dover Publications, 1975).
- 18 F. Wang, S. G. Johnson, and H. O. Everitt, "Maximizing performance of quantum cascade laser-pumped molecular lasers," *Phys. Rev. Appl.* **16**, 024010 (2021).